RESEARCH ARTICLE Received: 08 August 2019 | Accepted: 15 October 2019 | Online: 22 October 2019

JOURNAL OF GEOPHYSICS
Est. 1924
www.geophysicsjournal.com

Moon body resonance

Mensur Omerbashich[1,*]

[1)] Bosnian royal family, PO Box 1, Sarajevo, Bosnia

The full range of 50 initial, Moon-orbit-forced superharmonic resonance periods is detected in the 1969-1977 time-series of all 12474 consecutive 0.02 Hz moonquakes from the Apollo Program catalog. The resonance is found forcing the strongest-energy (highest-fidelity) part of the 10 hours–100 days (27.78–0.115741 μHz) long-periodic band at 99–67% confidence and below. Resonance signatures of the Moon's other four long tidal periods – synodic, anomalistic, nodical, and tropical – were also identified but not as separate drivers of body resonance. The spectra were computed using a least-squares spectral analysis method that enabled separation of the signal driver and noise signatures of all lunar tides, as well as extraction of the exact sequence of resonance periods affecting the solid Moon. As the main disruptive phase, the Moon's orbital period introduces nonlinearity into lunar vibration and thus forces lunar seismotectonics too, giving rise to superharmonic resonance and probably the so-called free librations as well. The spatiotemporally independent computations of Earth and Moon superharmonic resonances from seismicity time-series prove that (the magnification of) macroscopic mechanical resonance is from-quantum-to-macroscopic-scales universal, and therefore as important as gravitation and fundamental forces. I propose then that some of the craters and calderas in our Solar system are petrified evidence of polygonal Faraday latticing. Finally, since only planets with one moon are susceptible to resonance plate tectonics, to prevent Earth energy overload and disintegration, a global geoengineering scheme is proposed to reassign the smaller of Martian moons, Deimos, to Earth so to attenuate Earth plate tectonics while unlocking Mars plate tectonics for natural terraforming.

Key words—resonance computations, Moon tectonics, moonquake prediction, planetary physics, Mars.

1. INTRODUCTION

Plate tectonics is not the ultimate Earth theory (Jacoby, 2001), and it is not even understood why the Earth has plate tectonics (Stevenson, 2008). On the other hand, a computation of Earth's body (mechanical) resonance from global tectonic earthquakes has revealed resonance plate tectonics (Omerbashich, 2019a). A subsequent demonstration of Moon-body resonance from global moonquakes would then provide spatiotemporally independent proof of resonance tectonics and its universality.

Therefore, I proceed to identify the resonant tidal response of the Moon as a nonlinear system. Basically, in what follows, an attempt is made to detect the forcing period $T \in \Re$ that causes the Moon's own linear (tidal) response as well as any additional nonlinear vibration $n / (m\ T)$; $n \in \aleph$ – termed *subharmonic* for $n / m \in (0, 1)$; $n > 1 \wedge n \in \aleph$ or *superharmonic* for $n / m > 1 \wedge n / m \in \Re$ (Yang et al., 2016). Omerbashich (2019a) gave the basic methodology for identifying body resonance and parameters from the spectra of seismicity time-series.

The phenomenon of *resonating vibration*, or *resonance*, occurs when a physical system's natural period of oscillation coincides with another physical system's period of oscillation (or its fractional multiple). We then speak of *mechanical resonance* when the physical systems involve bodies of mass. Specifically, matching one system's natural period with another system's *subharmonic vibration* period or its fractional multiple gives rise to *subharmonic resonance*. Similarly, matching one system's natural period of vibration with another system's superharmonic vibration period or its fractional multiple gives rise to superharmonic resonance. Thus structural failure occurs in solids along a resonance period via frequency demultiplication – one of the rarest mechanical phenomena in Nature, known for its ability to magnify the energy injected at the fundamental disturbing frequency by 100s of times (Den Hartog, 1985).

Subharmonic and superharmonic resonances can develop in discrete parts of a physical system. As with all solids, the hundreds of tectonic plates and brittle regions in the upper mantle constitute Earth's vibrating parts, while those in the Moon remain elusive. Based on research finds from mechanical and electrical engineering, subharmonic resonances typically occur at periods shorter than (usually: fractions of) the long-periodic excitation; superharmonic resonances, at the periods longer than (usually integer multiples of) the long-periodic excitation. Most nonlinear systems will resonate at simple superharmonic resonant periods n / T as special case $m = 1$. Resonating linear systems are a special case of subharmonic resonators (Yang et al., 2016), which is a constraining factor in this research.

Since earlier spectral analyses of moonquakes occurrences – performed under the assumptions of Moon system's linearity or simple nonlinearity – found no periodicity other than a few tidal signals, here of interest is a strictly nonlinear (subharmonic and superharmonic) signal T_{Rsup}, as the only unexplored path. Proceeding in that direction requires looking into the long-periodic band commonly referred to as "long-periodic noise" that starts at the still unknown or largely uncertain natural period of vibration of the Moon. This band of interest then encompasses the *orbital* (likely the forcer phase) and *lunar-synodic month periods* (called physical periods), and the astronomical periods.

[*)] Correspondence to: hm@royalfamily.ba.

ARK:https://n2t.net/ark:/88439/x034508 2643-9271/19/63/0030/0042

Much like lunar forcing was considered part of the signal when demonstrating Earth-body resonance, here *geoforcing* (the Earth's forcing) of the Moon determines a critical part of the signal.

So in the following, I consider the Moon under nonlinear forcing as prescribed by the georesonator hypothesis, which I herewith tacitly assume applies to all macroscopic bodies of mass. Note again that, for resonant (nonlinear) components of vibration to occur, it does not matter where this nonlinearity originates – in the source mechanism, in the damping, or both (Den Hartog, 1985). Finally, to model the Moon as a fully nonlinear forced system in which one could expect anything, it is prudent to recall again that a single-frequency excitation always induces superharmonic resonances only (Yang et al., 2016).

2. Signal

In search of a complete sequence of Moon-body resonance subperiods (the signal), I consider all 13,058 seismic events in the 1981 (updated in 2008) *Levent.1008* Moonquakes Catalog of the Apollo Program's passive seismic experiment ALSEA, spanning the 1969-1977 Missions 11, 12, 14, 15, and 16, and sampled at the 0.02 Hz, or once-per-minute, rate (Nakamura et al., 1981); hereafter: the Moon Catalog. Catalog times were in Earth days, Earth hours, and Earth minutes (henceforth: days, hours, and minutes, respectively). The specific coverage was: 71 events from 1969, 624 from 1970, 1,912 from 1971, 3,007 from 1972, 1,896 from 1973, 1,376 from 1974, 1,087 from 1975, 1,612 from 1976, and 1,473 from 1977. Here the minor correction of 2018, Levent.1008c, was not used because the documentation did not specify corrections but did label them a priori as overall insignificant.

After the removal of 15 imprecisely time-stamped events and 569 time-duplicates (i.e., doublet, triplet, and quadruplet events with the same time-stamp, preventing time-series monotony), the remaining 12,474 seismic events were spectrally analyzed. Removing 4% of data was acceptable because, as shown for Earth-body resonance, omitting 2% of earthquakes from a much denser dataset did not affect the result adversely, and it could even be beneficial. Note here that the Earth demonstration relied upon 15 times fewer events that spanned less than half the interval of moonquakes used in here (Omerbashich, 2019a). Also, the selenophysics community relies extensively on the seismic observations from the ALSEA experiment; Khan et al. (2013) made an exhaustive review of those activities and studies. Past spectral analyses of deep moonquakes occurrences have claimed Moon's linear periodic responses, of ~13 days, 27 days, and 206 days periodicities; e.g., by Bulow et al. (2007) who used multitaper and spike-train spectral analysis methods.

3. Data Analysis

The spectra were computed using the Gauss-Vaníček spectral analysis (GVSA) method (Vaníček, 1969) (Vaníček, 1971), as $s_j^{GVSA}\left(T_j, M_j^{GVSA}\right)$; $j = 1\ldots\ k \wedge k \in \aleph$, with $k = 1000 \wedge k = 2000$ spectral resolutions. The GVSA falls in the Least Squares Spectral Analysis class of spectral methods that fit data with trigonometric functions. The GVSA is preferred over the Fourier class of spectral analysis methods (FSA) for analyzing raw records of unevenly spaced real data (Press et al., 2007). As variance-based, the GVSA provides a straightforward statistical analysis with a linear depiction of background noise levels (Omerbashich, 2004; 2006). GVSA is one of the most accurate methods of numerical analysis (Omerbashich, 2019b), enabling absolute accuracy, i.e., accuracy in extracting a period from big and raw data sets with 10s of billions of measurements, of down to twice the sampling rate (Omerbashich, 2004; 2007; 2019a; 2019b). The success of GVSA in geophysics has attracted a significant attention from the scientific community; for example, relevant research in and reviews of paleoclimate studies, such as by Smith (2007), Bailer-Jones (2009), Aberhan and Kiessling (2012), Baker and Flood (2015), and Erlykin et al. (2017).

The record contained over 7,000 tidal moonquakes as the dominant type, most of which were deep (below 650 km), and – as tacitly assumed – at least some shallow tidal events as well. Here data were not manipulated, unlike in the Fourier class of spectral analysis methods. Instead, spectral computations benefited from the GVSA's inherent ability to analyze raw data, as variance spectra thrive on the background or ambient noise. Sporadic seismic events, including around 1,700 meteorite impacts on the Moon's surface and about ten Lunar Module's touchdowns and booster firings, were left in the record since they all leave inharmonic signatures. Similarly, around 3,500 thermal events – driven by the change of day and night – were kept too; but since they leave harmonic signatures, those events were kept to boost spectral magnitudes by consolidating (overall tuning) the noise. Namely, given the Moon's said tidal lock with that same phase, equaling one Moon day, this day-night periodicity coincides with the signal driver and enhances it further. Here, polluting the signal by the day-night thermal events to the point of a biased result is not an issue since those events are mostly shallow and thus do not critically affect the whole-body resonance – specifically, the most energetic band that controls most of the mass and drives the body. Also, as in the Earth-body resonance demonstration, here too "driver" marks that (external) forcing phase that dominated the longest-periodic part of the Moon natural band. Likewise, the demonstration from seismicity occurrence (times) means direct detection of resonance as earthquakes occur ("ride on it"), not as they leave imprints onto some intermediary proxy – in which case secondary phenomena like day-night thermal induction could matter and would need to be accounted for as obviously affecting the analyses (here analyses include no proxies). Even if the Moon had an atmosphere comparable to the Earth's, day-night thermal variations (in fact: air molecules oscillations and corresponding gas resonances), do not carry sufficient power to excite the matter in its longest (of solids) band of vibration. Note also that the concept of adding noise to enhance the signal-to-noise ratio – known as stochastic resonance – has been demonstrated in many fields, including the application of the GVSA in geophysics (see Omerbashich, 2008). Finally, leaving meteorite impact events in moonquake records for signal enhancement is a standard procedure, e.g., in processing source waveforms.

Unlike the 1 Hz quality catalogs used to demonstrate Earth's body resonance, the Moon catalogs still lack a seismic magnitudes system uniquely related to source energy emissions. Thus, despite some attempts to define magnitudes, there is no consistent definition of moonquake magnitude (Nakamura, 2019). This regrettable circumstance half a century since the Apollo program confines one to spectral analyses of noisy time-series and prevents estimating the physically most likely cutoff-magnitude for defining energy levels of Moon resonance tectonics.

So to mimic earthquake records for the Moon, I arbitrarily assign to each event in the Moonquake Catalog a generic (random) seismic magnitude in undeclared units, from the [5.5, 7.5] interval. Although such magnitude range is physically unrealistic for the Moon as moonquakes likely are mostly in the M_w2-5 range, such a scale-up to mimic the case of the earthquakes is justified statistically since it helps spectral resolution to follow the boost in spectral magnitudes (from noise additions via keeping the meteorite-impact and day-night thermal events in the raw record). Most importantly, such an approach does not affect the signal itself because in the whole-body forcing the (longest-periodic segment of the) signal is overwhelmingly stronger than any noise signature or all the signatures combined (Omerbashich, 2019a). Same as for pure (complete) signals, strong noise signatures by the Moon's candidate forcers can be compared in-between also. Any other use of differentials in applied science works in the same way, say, the DGPS. This differential spectral analysis then makes the core of this paper. A convenient circumstance here is that all of the compared signals entertain mostly systematic noise and feature mutually like statistics.

Mimicking of earthquake records has been used to compile moonquake source spectra as well, so moonquakes' standard compressed plots are generic. Thus the signal envelope amplitudes for moonquakes are in millimetres on a standard plot as created by taking the absolute value of the difference between consecutive long-periodic data points, summing, and plotting them at a scale but in alternating polarities to give the appearance of a seismogram. (Nakamura et al., 1981)

As seen from the demonstration of Earth's body resonance, time-series of major catalogs of earthquakes possess a high degree of internal consistency, robustness, and ambiguity – as expected from data that describe a regularly but inconsistently driven physical process. As it turned out, those data indeed described a genuine, albeit nonlinear behavior of a physical system. (Omerbashich, 2019a) However, no such information can be expected from the moonquake data as those generally are of lower quality: overburdened with ambient and unknown noise, collected with unmaintained instruments, missing uniquely defined seismic magnitudes, and so on. Nonetheless, the moonquake data are uniquely ambiguous when taken as a whole, which suffices for spectral analyses in this (differential) demonstration of the whole-body resonance of the Moon by elimination.

Also looked into were the short-periodic spectral bands: 2'-15 days and 2'-100 days, which all returned active pure noise indicative of long-periodic excitation. Other inspected long-periodic bands included: 5h-30 days, 5h-60 days, 5h-100 days, 400'-100 days, 5h-150 days, and 5h-180, but results from those bands were found not as useful as the results from the primary band of interest, of 10 h–10 days.

The demonstration here differs from that of the Earth's case fundamentally as well because, unlike the Earth's natural mode, the Moon's natural period of oscillation is unknown or difficult to estimate at best. Estimates of the Moon mantle's viscosity vary greatly, and there are no reliable reference models of the Moon (Khan et al., 2013). Fortunately, thanks mainly to the Earth-Moon tidal lock, the Moon's orbital period (time to complete one orbit relative to stars; also called sidereal period), of T_M = 27.32166 days, is the only real candidate for the Moon's external forcing phase as well. Namely, the T_M introduces nonlinearity into the Moon's tidal response supposedly constantly while the already synchronized Moon keeps trying to resynchronize spatially with the ever-escaping Earth at precisely T_M. While this simple state of affairs indeed is a fortunate circumstance, it makes the demonstration here more laborious than for the Earth, because the Moon experiences several long-periodic tides so close to the orbital period that their potential for creating own long-periodic body resonance(s) must also be analyzed. Another fortunate circumstance here is that the Moon is overwhelmingly solid compared to the Earth so that the lunar physical setup itself prevents or minimizes significant loss of information due to lower data quality.

Thus another tidal period that could be reflected in (mixed with) the pure signal is the Moon's synodic month (time between two same lunar phases), of T_S = 29.53059 days. (By pure signal, I mean the moonquakes on a mathematically idealistic, uncoupled, and undisturbed body of mass so that all other Moon vibration is considered noise – unlike the classical view in which moonquakes are regarded to be the seismic signal.) Also, there are relevant astronomical lunar periods, which include:

- one *anomalistic month* (average time the Moon takes between two perigees; offset from the orbital period due to Moon's apsidal precession, of 8.8 years), of T_A = 27.55455 days,
- one *nodical month* (average time the Moon takes to return to the same node; offset from the orbital period due to Moon's nodal precession, of 18.6 years), of T_N = 27.21222 days, and
- one *tropical* month (average time of the Moon's crossing of the same equinox twice consecutively; slightly offset from the orbital period due to Earth's axial precession ("of equinoxes"), of ~26,000 years), of T_T = 27.32158 days (Seidelmann, 1992).

However, all these arbitrarily defined periods (with values averaged over the varying Moon's trajectory as due to various precessions) are of a considerable vertical pull – of up to a few dm – which normally hinders any secondary vibration so they cannot be expected to give rise to a (primarily horizontally-moving) long-periodic body resonance.

As surmised earlier, a variation in seismic magnitudes enables validation of a preset cutoff magnitude, and the corresponding physical process behind spectrally analyzed seismicity occurrence (Omerbashich, 2019a). An additional benefit from comparing the spectra of noisy moonquake v. impeccable M_w5.6+ occurrences records lies in revealing the physics of the extreme-energies band of the Moon. If such two dissimilar (presumably independent) datasets produce similar variance-spectra, then the working assumption here is that not only do those datasets describe a common astrophysical mechanism, but such mechanism could only arise due to the Earth-Moon resonating system. As mentioned in the above, missing unique moonquake magnitudes were simulated here. So if the Moon and the Earth variance spectra show resemblance, nature (and therefore type too) of seismic magnitudes will be irrelevant for establishing the existence and type of body resonance via differential spectral analysis that looks into different lunar candidate forcers. It would then be justifiable to use randomly generated seismic magnitudes. Based on what is known now on the Earth's body resonance and the variance-spectral response to that resonance, this reverse-engineering procedure is also helpful for determining the Moon's natural period of oscillation from real data. Unfortunately, as mentioned, a reliable whole-body selenophysical reference model from inversions is still missing due to sectored seismic coverage of the Moon and for other reasons.

While all bodies tend to synchronize (Pikovsky et al., 2001), the Moon has already attained its synchronization with the Earth, both spatially in the form of tidal (orbital-rotational) lock and temporally in the form of coupling of the natural periods of vibration at both macroscopic and quantum scales (Omerbashich, 2007). That is a fortunate circumstance for this demonstration, and one that takes away a degree of freedom from the Earth-Moon coupled oscillator. Thus Moon-body resonance, if its signature is present in moonquakes occurrences records, arises under nonlinear forcing due to the Moon orbital period's continuous attempts at resynchronization of the largely (but still not mutually entirely) synchronized Moon and Earth. Here also helpful is that the Moon overall is seismically comparable yet rather quiescent relative to Earth (Lorenz and Panning, 2018). This situation adds robustness to the temporal aspect of verifying the Earth-body resonance using moonquakes occurrences, as data density is significantly different than in the Earth case.

Although Moon seismicity lacks global coverage, a sectored coverage of the ALSEA experiment (that nonetheless snapped nearly half the Moon) suffices here because the seven-year data span from the relatively non-rotating Moon is enough to establish or rule out any nonlinear periodicities. Note again that the cyclic events due to the day-night thermal variation as a primary component of the Moon's ambient noise do not dominate the record. Furthermore, the absence of an atmosphere and so of atmospheric tides or gusty winds to account for in spectral analyses is of no particular benefit here because those tides would be a useful part of the signal. Namely, as with the demonstration of Earth's body resonance, here too, we deal with extreme energy bands to which those tides, if existed, would be a minor contributor. As with exploring the Earth's body resonance, here as well, I tacitly assume that all spectral estimates at different confidence levels are physically meaningful if at least 67% reliable. The success of the methodology applied by Omerbashich (2019a) justifies such an approach.

As outlined in the above, that success can be applied oppositely as well, in a bona fide twist. Since the data are of an undeclared but likely low quality, I regarded that vital shortcoming as an attribute which I then pushed to the fullest extent – by actually contaminating the data with the record's complete information and then looking not just for the parts of the signal above but also those below the 67% significance level. While not justified from the strict statistics point of view, this is justified from the physics point of view because the physical process of resonance seismotectonics has already been demonstrated for the Earth and found to be statistically significant. Then detecting even such a process's noise signature (of course alongside at least partial detection above a significance level) on another astronomical body in that body's long-periodic band would strongly indicate if not verify the presence of the same phenomenon on that other body as well. Conversely, the detection of resonance seismotectonics in the noisy record of moonquakes occurrences would add both extraterrestrial (methodological) and statistical (robustness-wise) credibility to the Earth resonance seismotectonics as demonstrated earlier from impeccable datasets. In other words, the proof of planetary resonance seismotectonics would then be complete. Undoubtedly, the Fourier class of spectral analysis methods is useless for the above approach to treating noisy natural datasets that cannot be denoised to any degree of ready-made utility.

Indeed, the preliminary spectrum on Figure 1 shows that, as variance percentage levels went down in absolute terms by more than an order of magnitude relative to Figure 2 in (Omerbashich, 2019a), the resemblance of the Earth spectra is remarkable. At the same time, the significance of each of the preliminary spectral magnitudes has indicated that there is only one superharmonic resonance of the solid Moon, Figures 2 and 3. Moreover, since a solitary superharmonic resonance always implies a single-frequency external forcing (Yang et al., 2016), further investigations to identify the period that forces the Moon resonance and seismotectonics are justified. Subsequently, I computed the spectrum of moonquakes occurrences, Figure 4.

Recall that statistical fidelity $\Phi > 12$ in physical data indicates a physically meaningful result (Omerbashich, 2006). Since classical (ambient) noise here mainly became part of the signal – causing spectral magnitudes to drop an order of magnitude or more from the Earth-body resonance demonstration – the fidelities that define the strongest-energies subband (here the ten $\Phi \geq 1$ lead periods of a resonance train) also dropped a magnitude of order. Thus a signal with $\Phi \in (\sim 1, \sim 12)$ can now be considered physically significant for the Earth-Moon physical system. By the same standard (considering the Earth and the Moon a single oscillator), the infinitesimal fidelities $0 \lesssim \Phi < 1$ shall define the signal's imprint in noise.

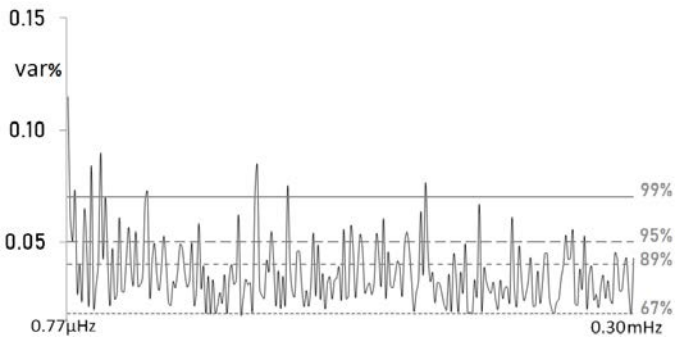

Figure 1. A preliminary spectrum of the moonquakes occurrences, computed for testing purposes in the Earth's natural band, 54'-15 days. While spectral magnitude response decreased an order of magnitude or more in absolute terms, a clear resemblance of the variance-spectrum of earthquakes occurrences from Omerbashich (2019a) strongly indicates that the superharmonic resonance drives the Moon seismotectonics too, and thus warrants further investigation. The spectral resolution used was k = 1000 points (lines). Corresponding spectral periods, matched to the orbital period-driven body resonance, are depicted per significance level in Figures 2 and 3 (stacked).

Let us note again that statistical fidelity of $\Phi > 12$ generally indicates a physically meaningful result for analyzing natural data sets (Omerbashich, 2006). Here, fidelity in the longest part of the 10 h–100 days band was increasing and at the longest detected period, of 89.3 days, has reached $\Phi = 1924.8 >> 12$. On the other hand, fidelity became practically 0 (falling below the 10^{-1} labeled precision) shortly after the 50^{th} subperiods of theoretical sequences (the series of resonance-forcing period's subperiods). Since $\Phi \in (\sim 1, \sim 12)$ characterized the most energetic resonance subband (as defined by the examined potential forcer-periods up to the 10 h high-ends), while taking on infinitesimal values (1, 0) beyond the 11^{th} subperiods in most of the sequences, that subband has defined the common strongest-energies subband as used in this paper.

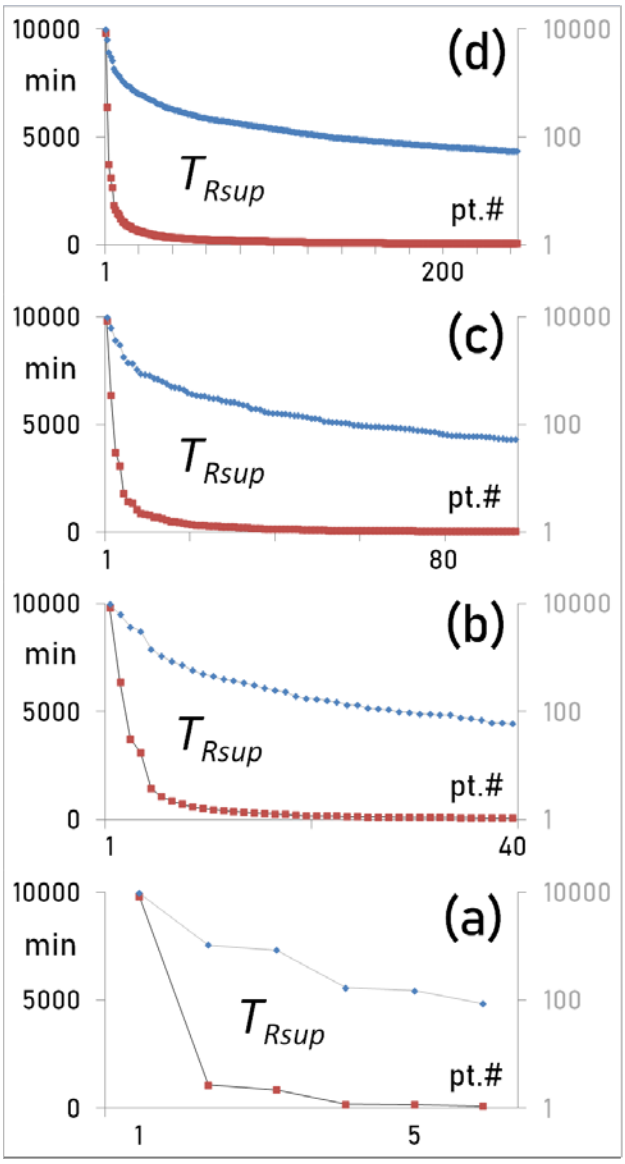

Figure 2. Significant periods in the preliminary spectra of 1969-1977 moonquakes' occurrences, Figure 1, per confidence level, in minutes: above 99% level (panel a), 95% (b), 89% (c), and 67% (d). The depiction's similarity with the earthquakes analysis of (Omerbashich, 2019a) prompted further investigation into the matching of the Moon's supposed theoretical superharmonic resonance subperiods T_{Rsup} with respective nearest most significant spectral periods. The supposed T_{Rsup} in minutes (dark line) shown stacked against the same along the logarithmically scaled ordinate (light line), offset for legibility.

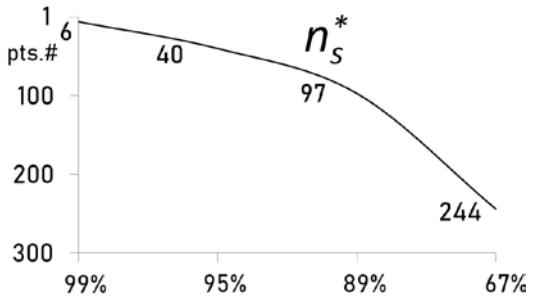

Figure 3. The overall number of statistically significant spectral points (lines) from the preliminary spectral analysis, Figure 1, per statistical significance level. The depiction's dissimilarity with (i.e., a steady change as seen here v. incoherent change as seen in) the same from earthquakes analysis by Omerbashich (2019a) indicates spectra of driven dynamics, i.e., a physical system in forced motion such that the system's vibration spectrum is insensitive to the choice of spectral resolution. The same for the Earth case had indicated a fully nonlinear physical system there – as due to rotating Earth's conjunctions in addition to the Moon-driven phase of the Earth. The stated dissimilarity then reflects a relative simplicity of the Moon case since the Moon, being spatially (tidally) locked to the overwhelming Earth, is not affected by the conjunctional component of nonlinearity. That and the internal similarity of Figure 2 panels prompted further investigation into the matching of the Moon theoretical superharmonic-resonance subperiods with the nearest respective spectral periods. For this, I double the spectral resolution and broaden the search for the solid Moon's driver phase to account for all lunar tides. Since additional periods are to be considered here also, by sliding the band's boundaries empirically, I selected the 10 h (27.78 μHz) cutoff for the boundary of the Moon's natural band. This approach to separating the free- from forced-oscillation bands of the Moon can be considered safe due to the lack of Moon reference models.

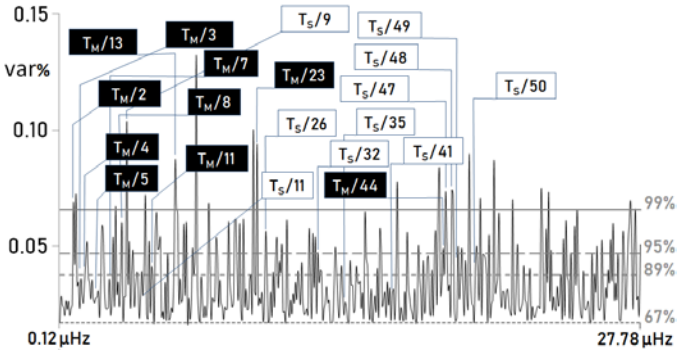

Figure 4. The spectrum of significant periods in all 12,474 occurrences of consecutive moonquakes from Day 208, 1969–Day 273, 1977. Spectral magnitudes are in percentage variance (var%), and resolution k = 2000 points (lines). Values corresponding to the depicted spectral peaks and theoretical superharmonic resonance subperiods are in Tables 1 and 2. Labels are non-arbitrary, here attached to the cases of two physical lunar tides. Thus the highlighted labels mark the superharmonic resonance subperiods as driven by the Moon orbital (sidereal) period, and the transparent labels the noise signature of the superharmonic resonance subperiods as driven by the synodic period. The depiction is a visual pseudo-separation of the orbit-forced signal v. synodic-forced noise. The 27.78 μHz cutoff was selected empirically, Figures 3 and 4, while the lower end was selected arbitrarily. That the used methodology and data treatment were justified is seen from the boost in all significant periods relative to the preliminary testing results of Figure 1. Note that the Moon orbital period, as used in this study, is not be confused with a selenocentric orbital period.

4. Discussion

I detected all of the fifty initial periods of a resonance subperiods-sequence as forced by the Moon's orbital phase, Table 1. Since the exact value of the Moon's natural period of vibration is unknown or highly uncertain at best, fifty is considered to be a sufficient sample size according to the law of large numbers. Besides – from the physics point of view – it made sense to look only for the first 32 significant superharmonic resonance periods since already the 33rd was shorter more than twice the band's upper end and below significance (where most of the signal's noise imprint was).

The Moon resonance's driven periods are the computed spectral periods that best match the corresponding theoretical subperiods in strongest resonance-energies (the longest-periodic part of the subband). Here I selected the first (longest) ten theoretical resonance periods as the cutoff for the strongest energies since the analyses have shown that statistical fidelity beyond the 11th resonance period drops an order of magnitude, and by several resonance periods beyond the 51st drops to practically 0. The performance of each candidate resonance-period is in Tables 3-5. Also, astronomical periods matched theoretical subperiods to a higher degree of internal consistency (Figure 6) than physical periods did (Figure 5). Such agreement was expected, because of the arbitrariness of astronomical periods, as opposed to the physical periods that represent the Moon more faithfully than the former ever could (except by sheer coincidence, as also shown here).

As seen from the matching of theoretical resonance subperiods against the corresponding nearest spectral periods computed at k = 2000 point (lines) resolution, the tropical period's relatively better performance in (i.e., its 50%-match with) the strongest-energies portion of the band than any other astronomical period's, Figure 4 and Table 3, is by chance. For if it were physically meaningful, then the other two arbitrary (astronomical) periods – anomalistic and nodical – would also perform in a like manner instead of failing. Besides, all five theoretical resonance periods in the longest part of the band, which were matched by the tropical period's resonance subperiods, Table 2, were also matched by the corresponding 5 of 7 orbital subperiods, Table 1, rendering all five of the strongest tropical subperiods as ghosts. The same can be seen for the nodical period also: all three of its matched resonance subperiods, Table 2, were also matched by the corresponding 3 of 7 of the orbital subperiods, rendering all three of the strongest nodical subperiods as ghosts too, Table 1. Finally, the number of overall matched periods (regardless of significance) in the tropical period's matching is still worse than in either the orbital or synodic periods', Table 3.

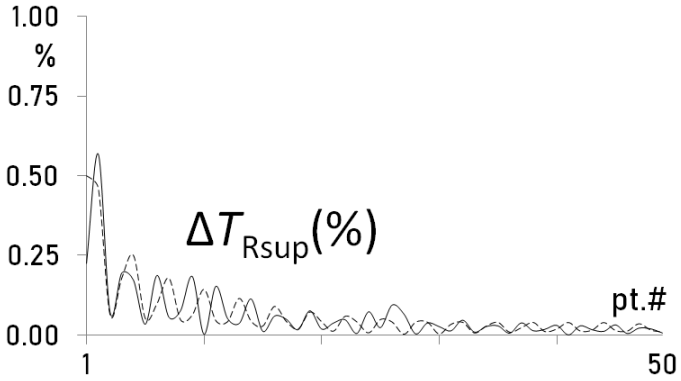

Figure 5. Relative match (Δ) of physical Moon-tidal periods' theoretical superharmonic resonance subperiods, with nearest respective periods from the computed spectra of moonquakes' occurrences, Figure 4, in % to the theoretical value. Shown are orbital period's matchings (solid line) v. synodic period's matchings (dashed line). The matchings stay well within 0.5% and below 0.1% most of the time.

Importantly, due to a relatively small difference between the orbital and tropical period, the orbital period excites not only the five strongest periods but 43 out of 50 of those in total. Finally, the orbital period outperforms other periods in the sense of average percentage-difference (percentage-matching), too, see Table 4. Note also the astronomical periods' internal consistency outperforming the same of the physical (orbital and synodic) periods, Figures 6 v. 5. Since astronomical periods dominate noise, this consistency translates into interference which forbids that precession-driven resonance – such as that induced by the tropical period – spills over into signal and becomes the driver of seismotectonics on the Moon (or the Earth as speculated in the past) as part of the Earth-Moon oscillator. The effect of astronomical periods on Moon's long-periodic information amounts to no more than ripples in selenophysical ambient noise.

As a critical verification of the above result against known physics of the Moon, note that, of the five Moon tides, the anomalistic and nodical were found to be least involved in the generation of Moon's body resonance, Table 2. This find was to be expected, given those periods' amplitudes of ~0.1 m that make them the two relatively largest vertical tides on the Moon (Seidelmann, 1992). They thus hinder any secondary vibration, including their own. Note also that body resonance primarily entails horizontal movements, as due to nonlinearity from external phase disturbance. Then in the absence of external forcing beyond the here examined lunar tides, the Moon body resonance as computed herein is the likely culprit behind the Moon's "free" librations as well, which are thus made effectively unceasing.

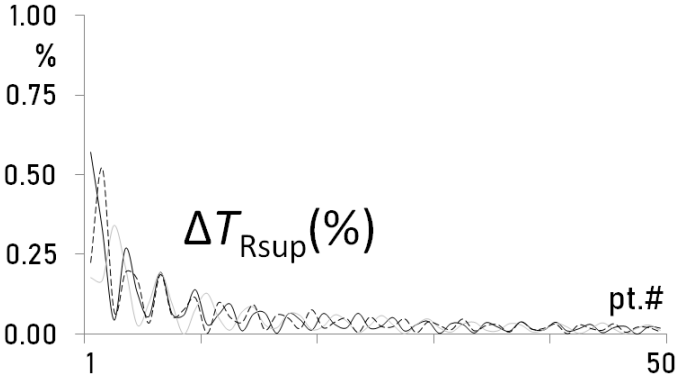

Figure 6. Relative match (Δ) of the astronomical tidal periods' theoretical superharmonic resonance subperiods, with nearest respective periods from the computed spectra of moonquakes' occurrences, Figure 4, in % to the theoretical value. Shown are anomalistic period's matchings (dark line) v. nodical period's matchings (dark dashed line) v. tropical period's matchings (light line). The matchings stay well within 0.5% and below 0.1% most of the time.

The discovery of the overwhelming spectral response of the occurrences of moonquakes to the orbital phase's resonance subperiods verifies the well-known harmonically induced lunar seismotectonics. As with the Earth, the detected superharmonic resonance of the Moon, $T_{\mathrm{Rsup}} = n / (mT)$, is of $n = T^2$ type, where $n / m \gg 1 \Rightarrow n \gg m$ characterizes the inducing process. In addition to revealing that seismotectonics universally is a resonance-induced process (even in particular cases of tidally locked inferiors like the Moon to the Earth), this research indicates that the Moon's synchronization with to it overwhelming Earth was, in fact, resonance-assisted (Thévenin et al., 2011). However, even as an indication, the find still validates the same definitive conclusion from the demonstration of Earth's body resonance.

	39343.19040	42524.04960	ORBITAL'S	32	Φ	Δ [min]	[%]	SYNODIC'S	34	Φ	Δ [min]	[%]
1/2	19671.59520	21262.02480	19627.43761		44.8	44.15759	0.224	21368.56952	*		-106.54472	0.501
1/3	13114.39680	14174.68320	13039.90940		19.8	74.48740	0.568	14109.20498		23.2	65.47822	0.462
1/4	9835.79760	10631.01240	9842.91332		11.3	-7.11572	0.072	10624.34487	*		6.66753	0.063
1/5	7868.63808	8504.80992	7853.33115		7.2	15.30693	0.195	8519.97869	*		-15.16877	0.178
1/6	6557.19840	7087.34160	6568.45564	*		-11.25724	0.172	7069.67606	*		17.66554	0.249
1/7	5620.45577	6074.86423	5618.56616		3.7	1.88961	0.034	6071.75853	*		3.10570	0.051
1/8	4917.89880	5315.50620	4908.70025		2.8	9.19855	0.187	5320.71496	*		-5.20876	0.098
1/9	4371.46560	4724.89440	4373.91357	*		-2.44797	0.056	4716.47660		2.6	8.41780	0.178
1/10	3934.31904	4252.40496	3931.33118	*		2.98786	0.076	4250.42821	*		1.97675	0.046
1/11	3576.65367	3865.82269	3570.08558		1.5	6.56809	0.184	3868.20039		1.7	-2.37770	0.062
1/12	3278.59920	3543.67080	3278.54214	*		0.05706	0.002	3538.61851	*		5.05229	0.143
1/13	3026.39926	3271.08074	3031.02032		1.1	-4.62106	0.153	3269.64186		1.2	1.43888	0.044
1/14	2810.22789	3037.43211	2811.67036	*		-1.44247	0.051	3038.66738	*		-1.23527	0.041
1/15	2622.87936	2834.93664	2621.92589		0.8	0.95347	0.036	2838.17280		0.9	-3.23616	0.114
1/16	2458.94940	2657.75310	2456.17209	*		2.77731	0.113	2656.62551		0.8	1.12759	0.042
1/17	2314.30532	2501.41468	2314.56898	*		-0.26366	0.011	2502.09481	*		-0.68013	0.027
1/18	2185.73280	2362.44720	2184.43419	*		1.29861	0.059	2364.55339	*		-2.10619	0.089
1/19	2070.69423	2238.10787	2071.71131	*		-1.01708	0.049	2237.18223	*		0.92564	0.041
1/20	1967.15952	2126.20248	1966.83407	*		0.32545	0.017	2126.58003	*		-0.37755	0.018
1/21	1873.48526	2024.95474	1872.06368	*		1.42158	0.076	2026.39860	*		-1.44386	0.071
1/22	1788.32684	1932.91135	1788.65870	*		-0.33186	0.019	1932.12694	*		0.78441	0.041
1/23	1710.57350	1848.87172	1709.93745		0.3	0.63605	0.037	1849.07115	*		-0.19943	0.011
1/24	1639.29960	1771.83540	1640.08364	*		-0.78404	0.048	1772.86165		0.4	-1.02625	0.058
1/25	1573.72762	1700.96198	1573.65434	*		0.07328	0.005	1700.28175	*		0.68023	0.040
1/26	1513.19963	1635.54037	1514.29834	*		-1.09871	0.073	1635.62909		0.3	-0.08872	0.005
1/27	1457.15520	1574.96480	1457.49135	*		-0.33615	0.023	1575.71312	*		-0.74832	0.048
1/28	1405.11394	1518.71606	1406.43276		0.2	-1.31882	0.094	1518.11575	*		0.60031	0.040
1/29	1356.66174	1466.34654	1355.77127	*		0.89047	0.066	1466.36374		0.3	-0.01720	0.001
1/30	1311.43968	1417.46832	1311.48258	*		-0.04290	0.003	1418.02382	*		-0.55550	0.039
1/31	1269.13517	1371.74354	1268.65816		0.2	0.47701	0.038	1371.20646	*		0.53708	0.039
1/32	1229.47470	1328.87655	1229.79647	*		-0.32177	0.026	1328.84623		0.2	0.03032	0.002
1/33	1192.21789	1288.60756	1192.06384	*		0.15405	0.013	1289.02482	*		-0.41726	0.032
1/34	1157.15266	1250.70734	1157.68942	*		-0.53676	0.046	1250.22150	*		0.48584	0.039
1/35	1124.09115	1214.97285	1124.19158	*		-0.10043	0.009	1214.91036		0.2	0.06249	0.005
1/36	1092.86640	1181.22360	1092.57776		0.1	0.28864	0.026	1181.53907	*		-0.31547	0.027
1/37	1063.32947	1149.29864	1063.63183	*		-0.30236	0.028	1148.85516	*		0.44348	0.039
1/38	1035.34712	1119.05394	1035.28938	*		0.05774	0.006	1118.96941	*		0.08453	0.008
1/39	1008.79975	1090.36025	1008.41820	*		0.38155	0.038	1090.59911	*		-0.23886	0.022
1/40	983.57976	1063.10124	983.70941	*		-0.12965	0.013	1062.69336	*		0.40788	0.038
1/41	959.59001	1037.17194	959.41766		0.1	0.17235	0.018	1037.07226		0.1	0.09968	0.010
1/42	936.74263	1012.47737	937.02515		0.1	-0.28252	0.030	1012.65752	*		-0.18015	0.018
1/43	914.95792	988.93139	914.95847	*		-0.00055	0.000	988.55383	*		0.37756	0.038
1/44	894.16342	966.45567	893.90721		0.1	0.25621	0.029	966.34562	*		0.11005	0.011
1/45	874.29312	944.97888	874.43726	*		-0.14414	0.016	945.11332	*		-0.13444	0.014
1/46	855.28675	924.43586	855.18971	*		0.09704	0.011	924.08444	*		0.35142	0.038
1/47	837.08916	904.76701	837.35299		0.1	-0.26383	0.032	904.64996		0.1	0.11705	0.013
1/48	819.64980	885.91770	819.68688	*		-0.03708	0.005	886.01610		0.1	-0.09840	0.011
1/49	802.92225	867.83775	802.75080	*		0.17145	0.021	868.13439		0.1	-0.29664	0.034
1/50	786.86381	850.48099	787.01433		0.1	-0.15052	0.019	850.35937		0.1	0.12162	0.014
1/51	771.43511	833.80489	771.38860	*		0.04651	0.006	833.87456	*		-0.06967	0.008

99% 95% 89% 67% * below significance

	39678.55200	39185.59680	39343.07520	ANOMAL.'S	37	Φ	Δ [min]	%	NODICAL'S	40	Φ	Δ [min]	%	TROPICAL'S	36	Φ	Δ [min]	%
1/2	19839.27600	19592.79840	19671.53760	19952.58890	*		-113.31290	0.571	19627.43761		44.8	-34.63921	0.177	19627.43761		44.8	44.09999	0.224
1/3	13226.18400	13061.86560	13114.35840	13182.63418	*		43.54982	0.329	13039.90940		19.8	21.95620	0.168	13182.63418	*		-68.27578	0.521
1/4	9919.63800	9796.39920	9835.76880	9924.01572	*		-4.37772	0.044	9763.12576	*		33.27344	0.340	9842.91332		11.3	-7.14452	0.073
1/5	7935.71040	7837.11936	7868.61504	7957.09863	*		-21.38823	0.270	7853.33115		7.2	-16.21179	0.207	7853.33115		7.2	15.28389	0.194
1/6	6613.09200	6530.93280	6557.17920	6604.47402	*		8.61798	0.130	6532.82800	*		-1.89520	0.029	6568.45564	*		-11.27644	0.172
1/7	5668.36457	5597.94240	5620.43931	5671.48064	*		-3.11607	0.055	5592.47746	*		5.46494	0.098	5618.56616		3.7	1.87315	0.033
1/8	4959.81900	4898.19960	4917.88440	4969.46051	*		-9.64151	0.194	4888.77567	*		9.42393	0.192	4908.70025		2.8	9.18415	0.187
1/9	4408.72800	4353.95520	4371.45280	4405.91423	*		2.81377	0.064	4358.08693	*		-4.13173	0.095	4373.91357	*		-2.46077	0.056
1/10	3967.85520	3918.55968	3934.30752	3970.20854		1.8	-2.35334	0.059	3918.54070	*		0.01898	0.000	3931.33118	*		2.97634	0.076
1/11	3607.14109	3562.32698	3576.64320	3602.11730	*		5.02379	0.139	3559.53456	*		2.79242	0.078	3580.69933	*		-4.05613	0.113
1/12	3306.54600	3265.46640	3278.58960	3305.53610	*		1.00990	0.031	3269.64186		1.2	-4.17546	0.128	3278.54214	*		0.04746	0.001
1/13	3052.19631	3014.27668	3026.39040	3054.07785	*		-1.88154	0.062	3015.84109		1.1	-1.56441	0.052	3023.41165	*		2.97875	0.098
1/14	2834.18229	2798.97120	2810.21966	2831.50046	*		2.68183	0.095	2798.60389	*		0.36731	0.013	2811.67036	*		-1.45070	0.052
1/15	2645.23680	2612.37312	2622.87168	2644.95737	*		0.27943	0.011	2610.55992	*		1.81320	0.069	2621.92589		0.8	0.94579	0.036
1/16	2479.90950	2449.09980	2458.94220	2481.47446		0.7	-1.56496	0.063	2451.17341	*		-2.07361	0.085	2461.19120	*		-2.24900	0.091
1/17	2334.03247	2305.03511	2314.29854	2332.49872	*		1.53375	0.066	2305.70708	*		-0.67197	0.029	2314.56898	*		-0.27044	0.012
1/18	2204.36400	2176.97760	2185.72640	2204.42484	*		-0.06084	0.003	2176.53908		0.6	0.43852	0.020	2184.43419	*		1.29221	0.059
1/19	2088.34484	2062.39983	2070.68817	2089.68356		0.5	-1.33872	0.064	2061.07559	*		1.32424	0.064	2071.71131	*		-1.02314	0.049
1/20	1983.92760	1959.27984	1967.15376	1983.02563	*		0.90197	0.045	1960.43124		0.4	-1.15140	0.059	1966.83407	*		0.31969	0.016
1/21	1889.45486	1865.98080	1873.47977	1889.68686	*		-0.23200	0.012	1866.26211	*		-0.28131	0.015	1872.06368	*		1.41609	0.076
1/22	1803.57055	1781.16349	1788.32160	1804.73981		0.4	-1.16926	0.065	1780.72514	*		0.43835	0.025	1788.65870	*		-0.33710	0.019
1/23	1725.15443	1703.72160	1710.56849	1724.62839	*		0.52604	0.030	1702.68544	*		1.03616	0.061	1709.93745		0.34	0.63104	0.037
1/24	1653.27300	1632.73320	1639.29480	1653.59406	*		-0.32106	0.019	1633.41088	*		-0.67768	0.042	1640.08364	*		-0.78884	0.048
1/25	1587.14208	1567.42387	1573.72301	1588.17980	*		-1.03772	0.065	1567.51017	*		-0.08630	0.006	1573.65434	*		0.06867	0.004
1/26	1526.09815	1507.13834	1513.19520	1525.80861		0.3	0.28954	0.019	1506.72082	*		0.41752	0.028	1512.39682	*		0.79838	0.053
1/27	1469.57600	1451.31840	1457.15093	1469.94301		0.3	-0.36701	0.025	1450.47038	*		0.84802	0.058	1457.49135	*		-0.34042	0.023
1/28	1417.09114	1399.48560	1405.10983	1416.35627	*		0.73487	0.052	1399.89398		0.2	-0.40838	0.029	1404.79235	*		0.31748	0.023
1/29	1368.22593	1351.22748	1356.65777	1368.09137		0.2	0.13456	0.010	1351.20825	*		0.01923	0.001	1357.29913	*		-0.64136	0.047
1/30	1322.61840	1306.18656	1311.43584	1323.00749	*		-0.38909	0.029	1305.79510	*		0.39146	0.030	1311.48258	*		-0.04674	0.004
1/31	1279.95329	1264.05151	1269.13146	1279.43961		0.2	0.51368	0.040	1264.66182	*		-0.61031	0.048	1268.65816		0.2	0.47330	0.037
1/32	1239.95475	1224.54990	1229.47110	1239.92488	*		0.02987	0.002	1224.79406	*		-0.24416	0.020	1229.79647	*		-0.32537	0.026
1/33	1202.38036	1187.44233	1192.21440	1202.77780		0.2	-0.39744	0.033	1187.36311	*		0.07922	0.007	1192.06384	*		0.15056	0.013
1/34	1167.01624	1152.51755	1157.14927	1166.66059		0.2	0.35565	0.030	1152.15216	*		0.36539	0.032	1157.68942	*		-0.54015	0.047
1/35	1133.67291	1119.58848	1124.08786	1133.71537	*		-0.04246	0.004	1120.00996		0.1	-0.42148	0.038	1124.19158	*		-0.10372	0.009
1/36	1102.18200	1088.48880	1092.86320	1102.57972	*		-0.39772	0.036	1088.62761	*		-0.13881	0.013	1092.57776		0.1	0.28544	0.026
1/37	1072.39330	1059.07018	1063.32636	1072.15328	*		0.24002	0.022	1058.95597	*		0.11421	0.011	1063.63183	*		-0.30547	0.029
1/38	1044.17242	1031.19992	1035.34408	1044.26564	*		-0.09322	0.009	1030.85887	*		0.34105	0.033	1035.28938	*		0.05470	0.005
1/39	1017.39877	1004.75889	1008.79680	1017.79198	*		-0.39321	0.039	1005.05222	*		-0.29333	0.029	1008.41820	*		0.37860	0.038
1/40	991.96380	979.63992	983.57688	991.81003	*		0.15377	0.016	979.70853	*		-0.06861	0.007	983.70941	*		-0.13253	0.013
1/41	967.76956	955.74626	959.58720	967.89878	*		-0.12922	0.013	955.61155	*		0.13471	0.014	959.41766		0.1	0.16954	0.018
1/42	944.72743	932.99040	936.73989	944.37227		0.1	0.35516	0.038	932.67150		0.1	0.31890	0.034	937.02515		0.1	-0.28526	0.030
1/43	922.75702	911.29295	914.95524	922.66862	*		0.08840	0.010	911.49630	*		-0.20335	0.022	914.95847	*		-0.00323	0.000
1/44	901.78527	890.58175	894.16080	901.94014	*		-0.15487	0.017	890.60223	*		-0.02048	0.002	893.90721		0.1	0.25359	0.028
1/45	881.74560	870.79104	874.29056	881.47697		0.1	0.26863	0.030	870.64460	*		0.14644	0.017	874.43726	*		-0.14670	0.017
1/46	862.57722	851.86080	855.28424	862.53899	*		0.03823	0.004	852.16434	*		-0.30354	0.036	855.18971	*		0.09453	0.011
1/47	844.22451	833.73610	837.08671	844.39764	*		-0.17313	0.021	833.87456	*		-0.13846	0.017	837.35299		0.1	-0.26628	0.032
1/48	826.63650	816.36660	819.64740	826.43622	*		0.20028	0.024	816.35339	*		0.01321	0.002	819.68688	*		-0.03948	0.005
1/49	809.76637	799.70606	802.91990	809.76708	*		-0.00071	0.000	799.55336	*		0.15270	0.019	802.75080	*		0.16910	0.021
1/50	793.57104	783.71194	786.86150	793.75707	*		-0.18603	0.023	783.94078	*		-0.22884	0.029	787.01433		0.1	-0.15283	0.019
1/51	778.01082	768.34504	771.43285	777.86515		0.1	0.14567	0.019	768.43566	*		-0.09062	0.012	771.38860	*		0.04425	0.006

Table 2: Differential Spectral Analysis of the Apollo Moonquake Catalog– Moon's astronomical tides: the difference Δ, or the match, in Earth minutes and % to the theoretical value, between theoretical resonance subperiods v. corresponding nearest computed periods from the spectra of moonquakes occurrences, Figure 4. The first ten subperiods are taken to possibly define the strongest-energies part of the energy band, as in Table 1, where the last 40 subperiods reveal the signal's imprint (if any) in noise as in Table 1. Matched were astronomical periods: anomalistic (dark gray background), nodical (gray background), and tropical (light gray background). All cases: the first ten subperiods reveal that the respective period is not driving the strong motion, while the last 40 reveal the respective signal's imprint in noise. (Note that all five tropical period's matchings and all three nodical period's matchings in the strongest energies are driven by the orbital period, Table 1, as the common source, making those 5+3 periods ghosts.) Below-significance matchings, marked with an *, are seen as always fitting the respective tidal period's resonant imprint in noise (i.e., each driver produces its sequence of resonant subperiods, but neither sequence affects the solid Moon, see Table 1 for the antithesis demonstration). The color scheme is as in Table 1.

Table 1 (FAR ABOVE). Differential Spectral Analysis of the Apollo Moonquake Catalog – Moon's physical tides: the difference Δ, or the match, in Earth minutes and % to the theoretical value, between theoretical resonance subperiods v. corresponding nearest computed periods from the spectra of moonquakes occurrences, Figure 4. Orbital period's matchings (dark background): 10 lead subperiods dominate motion in the strongest-energies subband defined by $\Phi \in (\sim 1, \sim 12)$ fidelity, where seven subperiods are seen to dominate the subband (driving the signal), while 40 final subperiods reveal the signal's noise imprint as defined by infinitesimal fidelity $0 \lesssim \Phi < 1$. Synodic period's matchings (light background): 10 lead subperiods reveal the period not driving the strong motion, and 40 final subperiods reveal the signal's noise imprint. Below-significance matchings, marked with a *, seen fitting the respective tidal period's resonant imprints in noise as every driver produces its sequence of resonant subperiods, but only the orbital period's sequence affects the solid-Moon vibration. By a match, I mean a spectral period nearby corresponding theoretical resonance subperiod, to within ±0.5% for the strongest-energies subband (the signal in the strict sense) and ±0.1% for noise. The criterion is based on the success of the Earth-body resonance demonstration that had set the precision for the Moon case an order of magnitude lower from the declared precision in the Earth case, of ±5%. This reasoning is justified by the overall variance (data quality) dropping also an order of magnitude for the Moon relative to the Earth case, Figure 1. Such a drop in variance meant that the Moon case had to be imposed higher stringency on than the Earth case – an order of magnitude or better.

The phenomenon of body (mechanical) resonance – demonstrated here as the Earth-Moon coupled mechanical oscillator – is universal by definition so that only planets with a single moon could feature plate tectonics. On the other hand, multi-moon planetary systems experience mechanical vibration interference, which commonly forbids resonance seismotectonics in solids. We see this in our Solar system, where the Earth is the only planet with one moon and the only planet with active plate tectonics. That this is no coincidence can be seen on the example of Venus, which early on probably had a moon (Alemi and Stevenson, 2006) with the possibility of a dynamo, i.e., own magnetic field (Stevenson, 1983). Venus had also seen the beginning of active plate tectonics (Basilevsky and Head, 2000) but, judging by its crustal recycling, possibly ending half a billion years ago (Arkani-Hamed and Toksöz, 1984), Venus could not sustain tectonics – probably due to losing its moon. So in addition to solid and dwarf solid planets without natural satellites, and thus no plate tectonics either (Mercury; Venus; Pluto; Ceres), the remaining solid (Mars) and potentially solid planets (Neptune) have more than one moon so that they have no plate tectonics either.

	T_O	T_S	T_T	T_A	T_N
	Overall				
No. of significant:	<u>18</u>	16	14	13	10
No. of insignificant:	<u>32</u>	34	36	37	40
	In strongest resonance energies				
No. of significant:	<u>7</u>	3	5	3	1
No. of insignificant:	<u>3</u>	7	5	7	9

Table 3. Performance of each of the Moon's long-periodic tidal periods of interest, in matching of their theoretical resonance subperiods with the corresponding nearest periods from the computed spectra of moonquakes occurrences, Figure 4, and Tables 1 and 2, according to the criterion of statistical significance (Yes/No) of the matched spectral period's peaks. The Moon's orbital period, T_O, as one of the two physical tides of the Moon (the other being the synodic, T_S) outperforms (underlined values) the synodic tide and all three astronomical tides (tropical, T_T; anomalistic, T_A; nodical, T_N) – both overall and in the strongest resonance energies subband, of 2.5-30 days (~0.4–4.6 μHz).

Then for the natural (over-time) terraforming to be geoengineered on a multi-moon planet like Mars, tectonics must first be activated and the resonating capability unlocked by removing (relocating or disintegrating) all the moons save for the resonance-wise most dominant one. Due to the sheer number of natural satellites per planet in our Solar system, Table 5, such terraforming of Mars is a most feasible choice for humans to create a backup mother planet, because it is guaranteed to succeed, and asteroid relocation is achievable (Fahnestock and Scheeres, 2008). Here, Deimos is the better candidate of the two moons for the elimination because it is significantly smaller than the Phobos and significantly farther from Mars already. Likewise, in an inverse geoengineering procedure, an outer astronomical body could be relocated (tractored or pushed) inside the Earth's vicinity and turned into the Earth's secondary moon. (Of course, when choosing the right orbit for a secondary moon, special care must be exercised to make that new satellite the Moon's inferior in terms of resonance capability, or else Earth plate tectonics could turn into a terraforming event causing a rapid Earth energy overload and disintegration, while life forms could lose their circadian rhythms.) In this way, Earth plate tectonics would be brought to a near halt before it alone sets off a terraforming event and the overload. The two geoengineering schemes could be combined into one by turning Deimos into the Earth's secondary moon directly so to reboot Mars plate tectonics while simultaneously quiescing the Earth's plate tectonics.

	T_O	T_S	T_T	T_A	T_N
$\sum\Delta$ (%)	3.13	3.26	2.83	3.05	2.64
No. of significant:	<u>18</u>	16	14	13	10
$\bar{\Delta}$(%)	<u>0.17</u>	0.20	0.20	0.23	0.26

Table 4. Performance from Table 3, but according to the criterion of average matching in percents (the differences between theoretical resonance-subperiods and corresponding nearest computed spectral periods). As in Table 3, the Moon's orbital tide is again seen outperforming (underlined values) all other periods. The average was taken over the matched spectral periods statistically significant if at least 67% significant. This performance revealed that the matching of the orbital period against the computed spectra of moonquakes not only outperforms other candidate forcers but is also physically meaningful. This performance has corroborated that considering both signal and its noise imprint together when extracting a physical process from natural data is valuable for low-quality records).

It is widely believed that Phobos and Deimos are asteroids captured by Mars, where Deimos was captured first (Cazenave et al., 1980), supporting a notion from the present study that adding of the second moon into the Martian system had brought plate tectonics on Mars to a near halt noticed by Yin (2012). Besides, both Martian moons have attained synchronous rotation (tidal lock) with Mars, as well as nearly circular orbits. According to the present study, that was due to their pivotal roles as On/Off tectonics switches via constantly injecting extra energy loads into Mars. This resonantly inserted excess-energy then gets redistributed tidally back to the satellites as their increasingly rough trajectories. Thus the initial, extremely elliptical orbits of captured asteroids-turned-moons get smoothed out ever so slightly over a long time to nearly perfect circles today. This setup is akin to the Earth-Moon coupled oscillator and the Moon's tidal lock on the Moon's own nearly circular orbit.

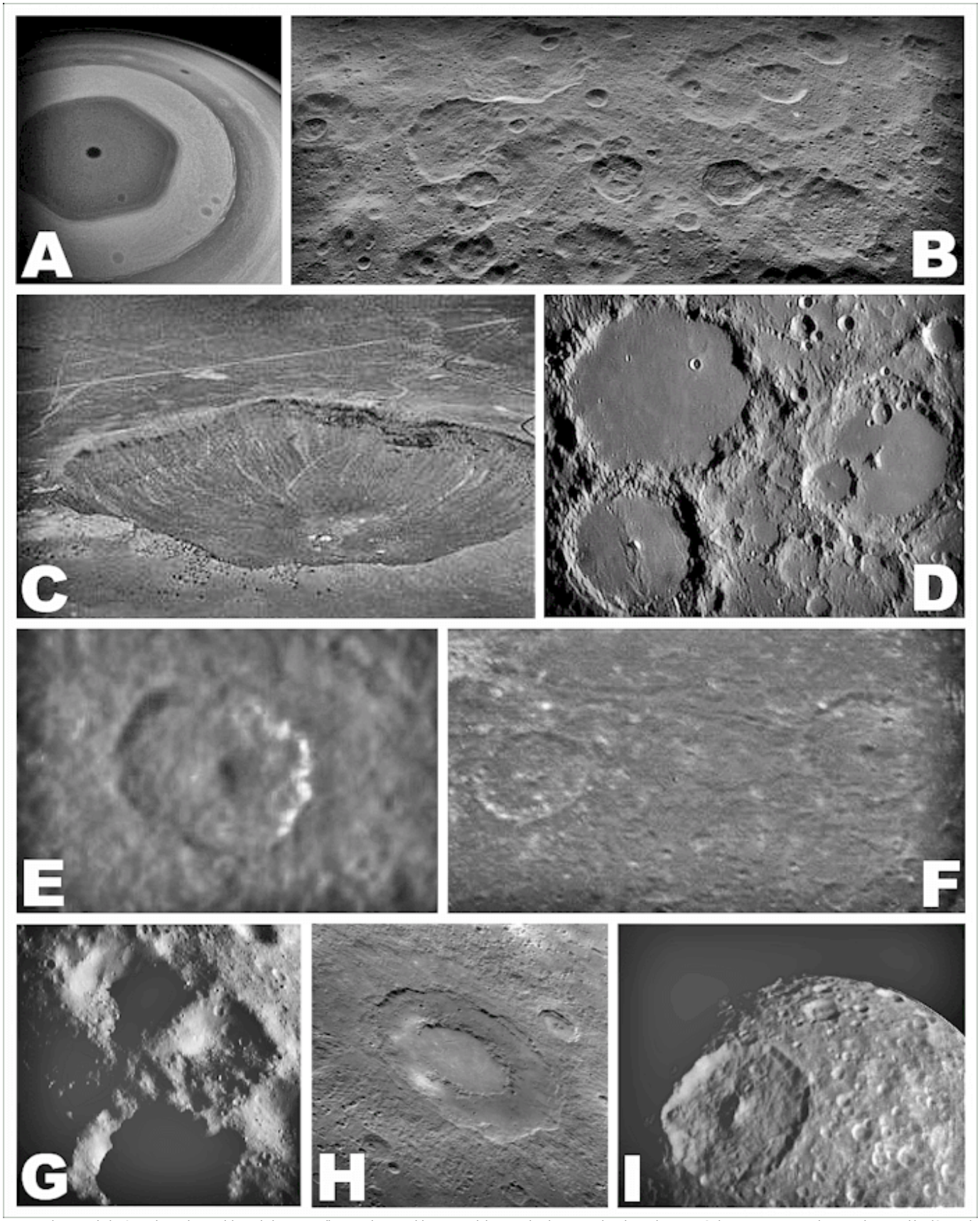

Image 1 (composite). Complex polygonal (mostly hexagonal) "cratering", "calderas", and the ongoing jet streaming throughout our Solar system: A. persistent polar-zonal jet (Saturn); B. Ahuna Mons (Ceres); C. Barringer Crater (Arizona, USA); D. Ptolemaeus Craters (Moon); E. planform on Saturnian moon Tethys; F. planform on Uranian moon Ariel; G. tetragonal planform (asteroid Eros); H. Rachmaninoff Crater (Mercury); I. Herschel Crater (a Saturnian moon Mimas). Many other bodies also feature traces of complex planforms. Ceres alone has 258 polygonal "craters", most or about one-half of which are hexagonal (Otto et al., 2016). The polygonal standing wave was first demonstrated in the 17th century by Hooke. Thanks to the demonstration improvements separately by Euler, Riccati, and Chladni in the 18th century, as well as Faraday in the 19th century, it can be shown empirically that, depending on the object of study, at specific frequencies or their integer multiples, the sum-form from all the (standing) waves on that object's surface takes shape of a solitary square, a solitary pentagon, a solitary hexagon, a solitary heptagon, or a solitary polygon with yet more angles, or even an asymmetric solitary polygon. Note *superhexagons* – the adjacent (hiving) and hexagons inside hexagons (including inner domes as not fully developed inner hexagons), see Figure 7. Scales vary, as ~1-1000 km across an image (B – I).

Planetary body	**Mercury**	**Venus**	**Earth**	**Mars**	**Jupiter**	**Saturn**	**Uranus**	**Neptune**	**Ceres**	**Pluto**	**Haumea**	**Makemake**	**Eris**
body type	planet	planet	planet	planet	planet	planet	planet	planet	dwarf	dwarf	dwarf	dwarf	dwarf
body state	solid	solid	solid	solid	gaseous	gaseous	gaseous	solid?	solid	solid	gaseous	gaseous	gaseous
number of moons	0	0	1	2	79	62	27	14	0	5	2	1	1

Table 5. The number of presently known moons per planet of our Solar system (unlikely to change significantly). Ordered left-to-right with increasing mean distance from the Sun. The "solid" and "gaseous" labels refer primarily to the body surface. The planetary classification and moon count is per the International Astronomical Union. Moonlets are omitted, as likely negligible for macroscopic considerations of this study that already account for all the moons. Also, single-moon dwarf planets lack mass and diameter for sustained resonance plate tectonics there.

Finally, supposed impact cratering (or calderas eroding) of complex polygonal – primarily hexagonal – shapes, is found throughout our Solar system (Otto et al., 2016), see Image 1. Also, the spatial clustering, as shown in the number of moons in Table 5, is due to the Sun and Jupiter absorbing or clearing most moons of the proto Solar system. At that time, 3-4.5 billion Earth years ago, the surface of all planets and moons likely was molten, as testified by the polygonal cratering (van Dijk and Kistemaker, 1981). Note here that the detailed mechanism of collapse (of craters supposedly circular or oval on impact; but by analogy also: of volcanic calderas sinking or eroding) is still not fully understood because straightforward use of standard rock mechanics models does not predict the (polygonal) type of collapse observed (Melosh, 1996). Then observations of such alleged proto cratering, or contemporary polygonal dynamic flows such as Saturn's persistent polar-zonal hexagonal jet (Godfrey, 1988), support the alternative notion of a Solar system-wide, resonance-assisted macroscale dynamic. This dynamic occurs as planets suffer natural vibrational disturbances due to conjunctions in the virtually coplanar Solar system (Omerbashich, 2019a). For example, the Saturn's hexagonal jet – which is larger than the Earth in diameter – is a stationary planetary wave, as many have claimed. However, just as the Solar system-conjunctions-driven (appearing as the Moon-only-driven) main motion of the Earth tectonic plates takes east-west preferential orientation, so is the Saturn's polar jet being forced zonally and continuously by the conjunctionally induced disturbances to nonlinear vibration, rather than being due to internal planetary reasons as thought by some. Besides, local conditions would need to coincide spatiotemporally a whole lot for a single localizing explanation to hold universally. Then a common, Solar-system explanation of the standing-wave morphology is called for instead; this requires that (magnification of) mechanical resonance be a cross-scale morphological phenomenon like gravitation and physical forces.

The presence and spatial density of polygonal, primarily hexagonal, cratering on such a small body as Ceres, is surprising. That, and the presence of adjacent polygons as well as polygons within polygons – like in Image 1-B, D, and G (dwarf planet Ceres, the Moon, and asteroid Eros, respectively) – are pointing at the conclusion that the polygonal morphology represents neither crater collapsing nor calderas eroding, but a lattice of standing waves instead. Such polygons, including *superhexagons* (the hiving; hexagons inside hexagons), can be reproduced experimentally in hydrodynamic studies of Faraday instability, e.g., by Tse et al. (2000), who also demonstrated that superharmonic vibration destroys the standing hexagons, see Figure 7. Here continuous superharmonic resonance was found in both Earth and Moon seismicity records examined. If at least some of the traces of supposed craters and calderas are, in fact, Faraday lattices, then the relatively good condition of polygonal morphology as found on Ceres, the Moon, and other bodies reflects the fact that the Solar system bodies once were fire-balls enveloped in molten material. The polygonal morphology has remained densely packed and grouped into adjacent cells, but isolated enough to dismiss Rayleigh thermal instability. In its various episodes, the resonance had to stay active over a long time until loss of heat enabled solidification (hydration absent). As a result, this activity remains fossilized for us today as arrays of standing hexagons and other polygons. Moreover, if the Ceres had remained resonantly excited for that long, its patterning represents pristine evidence of permanent mechanical-resonant interactions among the Sun and its coplanar companions. Then the only reason why today we do not see the creation of standing-hexagon meshes is that there are no astronomical bodies with molten surfaces in the Solar system at present. An example, even unrelated to cratering, of morphology-driving superharmonic resonance on an astronomical body, is in Image 2. Finally, resurfacing observed on planets with plate tectonics like the Earth is also found on planets without plate tectonics like Venus, requiring an alternative mechanism (Strom et al., 1994).

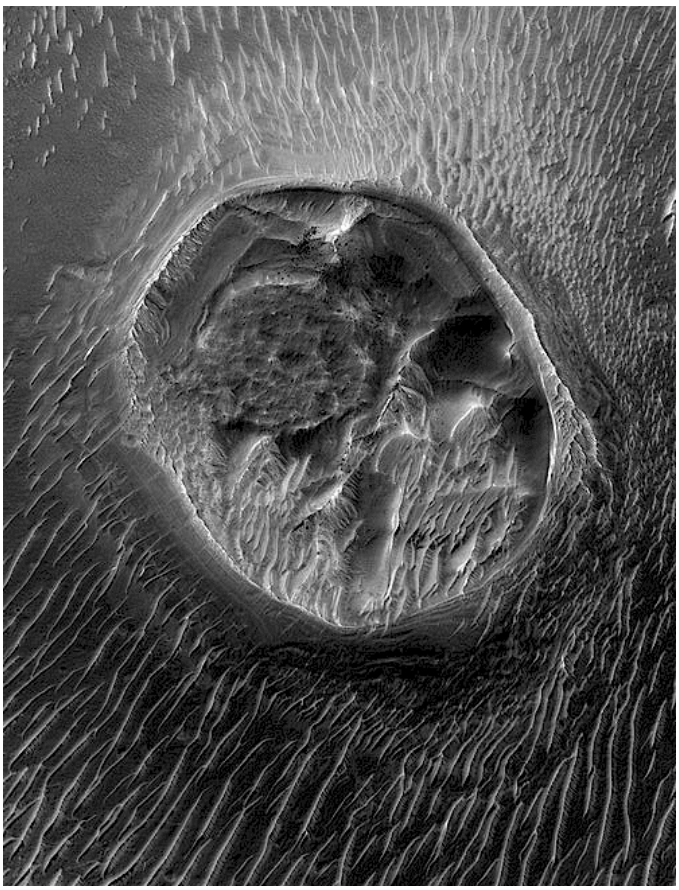

Image 2. A mesa in Noctis Labyrinthyus on Mars, surrounded by extensive fracturing of Valles Marineris. Scale: 0.4 km across the mesa. As plate tectonics never developed on Mars, the nonetheless systematic morphology has a standing hexagon inside a Faraday pattern and – in the absence of evidence of impact cratering – indicates the Solar-system-wide superharmonic resonance shaping the topography on astronomical bodies.

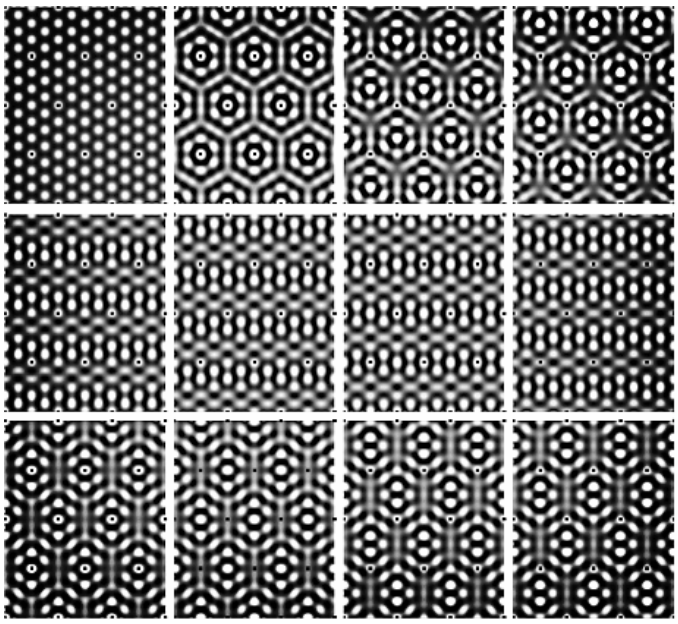

Figure 7. Experimentally reproduced nonlinear dynamics at the free surface of a horizontal layer of fluid under vertical vibration (single-frequency forcing), showing a spontaneous generation of Faraday (standing) waves of regular shapes, where "subharmonic vibration breaks standing hexagons" (Tse et al., 2000). It can be shown that similar patterns emerge under multi-frequency forcing as well. The analogous concept in the present research is that of a rotating astronomical body whose masses get stirred by gravity vectors (tides), while its planetary conjunctions in the Solar system's plane induce nonlinearity in that body's vibration, and thus resonance too. The top and bottom rows depict superhexagons – adjacent (hiving) and hexagons inside hexagons (including inner domes as not fully developed inner hexagons). Throughout our Solar system, the experimental superhexagons are comparable to many "craters" and "calderas", see Images 2-B, D, E, F, H, and I. Since harmonic mechanical resonances destroy standing hexagons, these gigantic (kilometre-scale) polygonal planforms by now are erased from Earth by resonances due to the first few of rT_M, $r \in \aleph$ lunar tides. Other solid planetary bodies in our Solar system (see Table 5) without any or with two or more moons (where such resonances are thus absent) still feature petrified, spatially relatively dense polygonal planforms such as those depicted in Image 1-B through I, and Image 2. Note that in the above, what Tse et al. (2000) termed subharmonic vibration, is a special case of $r = 2n^{1/2}$ of the $n = T^2$, $n \gg m \wedge m \in \aleph$ superharmonic vibration that I report in here and in the Earth-body resonance demonstration. Thus the presence of polygonal-planiform morphology throughout our Solar system is living proof of conjunctionally induced continuous nonlinear vibration on astronomical bodies as a universal phenomenon. This nonlinear vibration gets significantly affected on solid planetary bodies with a single moon: **spatially** – from attenuation to complete stop, and **temporally** – from enhancement via resonance magnification, to disintegration. This spatiotemporal aspect of the phenomenon of conjunctionally induced resonances is useful as a diagnostics tool for assessing the state of a planet's spatiotemporal stability. By how far a body is from losing its hiving and other environmental patterns – the same body is as near its disintegration as well.

Also, geophysical non-Newtonian flows that form polygonal patterns are common on Earth. For instance, hexagonal patterns in salt deserts are a global phenomenon with an unknown driving mechanism, while their length scale does not change much from Chile to Iran to the West coast of the US – even though the environmental circumstances change drastically. So the mechanism that causes those patterns has to be rather robust to changing circumstances for it to express the same length scale and shape in a variety of surroundings on several continents (Lasser, 2019). Thus, in addition to the above global kilometre-scale polygonal planforms throughout our Solar system, this strongly-global scaling of polygonal geophysical patterns (albeit along metre-scales only) reveals an incessant global vibration that had been met by a local resonant response. This global vibration is due to conjunctionally induced vibrational nonlinearity and is attenuated by a single-moon forcing, which scales down any Faraday patterning by (on Earth: three) orders of magnitude, before finally succeeding to thwart it entirely.

5. Conclusions

Using spectra of moonquakes occurrences, I was able to verify that lunar seismotectonics arises in the harmonic response of Moon's inner regions ("tectonic plates"; bodies of mass) to the (range of at least 50 initial) superharmonic resonance periods shown fully recoverable from the cataloged moonquakes occurrences. Thus same as with tectonic earthquakes, tectonic (tidal) moonquakes too were captured as they "ride" on the resonance. The T_M phase drives moonquakes and probably excites the so-called free librations of the Moon as well. The successful computational demonstration of the Moon's superharmonic resonance is supported additionally by a vast morphological presence of petrified or streaming Faraday standing waves (mostly hexagons) in our Solar system. Unlike the Earth, where resonances due to rT_M, $r \in \aleph$ lunar tides, erased its kilometre-scale polygonal morphology, solid planetary bodies without any or with two or more moons still feature a rich such morphology.

As with the Earth, the detection of the Moon's virtually entire resonance range means that lunar resonance is unceasing and that all of the Moon's inner regions respond actively to some of the resonance periods as those activate. Same as the Moon gives rise to the long-periodic resonance of the Earth, the Earth gives rise to the long-periodic resonance of the Moon as well. This revealed a coupled mechanical oscillator made of the two bodies, in which the inferior body has attained the absolute synchronization, i.e., both spatially (orbital) and temporally (vibrational), while the superior body has attained a relative (temporal, i.e., vibrational) synchronization of 1 h (Omerbashich, 2019a). The fact that the Moon is under a single external forcing makes moonquake prediction considerably simpler than earthquake prediction, pending quality lunar data.

The universality of spatiotemporally-independently verified (magnification of) mechanical resonance enables geoengineering undertakings on planetary scales and beyond. Tectonogenic mechanical resonance arises on solid planets with one moon (which generally also tends to destroy any Faraday standing hexagons). It follows that long-repressed plate tectonics on Mars can be revived – by removing one of that planet's two moons. Moreover, assigning an outer astronomical body to the Earth as her secondary moon (a Moon's inferior) would significantly restrain and altogether forbid Earth plate tectonics to set off a terraforming event that, if unchecked, would end in global energy overload and Earth disintegration. Since active sonorous tectonics is critical for life to emerge on an astronomical body, the unlikelihood of having precisely one moon is a constraint for a planet to have active geophysics and thus complex, cross-scale-synchronously vibrating biochemical forms able to sustain life. Along with, or instead of, gravitation and physical forces, the (magnification of) mechanical resonance is a vital natural phenomenon previously ignored in macroscopic studies.

Acknowledgments

I thank Dr. Ralph Lorenz and Dr. Yosio Nakamura for valuable discussions and suggestions, Barbara Pope (NASA-NSSDCA) for help with the data, and Dr. Spiros Pagiatakis for his software LSSA v.5.0. Corrections by the reviewer Dr. Aggeliki Barberopoulou were most useful. This paper is part of a paper doublet along with Earth body resonance, *J. Geophys.* 63(1):15-29.

References

Aberhan, M., Kiessling, W. (2012) Phanerozoic marine biodiversity: a fresh look at data, methods, patterns and processes. In: *Earth and Life* (Ed. Talent, J.), Intl. Year of Planet Earth book series, pp.3-22. ISBN 9789048134274

Alemi A., Stevenson, D. (2006) Why Venus has no moon. In: AAS/Division for Planetary Sciences Meeting Abstracts 38. *Bull. Am. Astron. Soc.* 38:491

Arkani-Hamed, J., Toksöz, M.N. (1984) Thermal evolution of Venus. *Phys. Earth Planet. Inter.* 34:232-250

Bailer-Jones, C.A.L. (2009) The evidence for & against astronomical impacts on climate change & mass extinctions: a review. *Int. J. Astrobiol.* 8:213-219

Baker, R.G.V., Flood, P.G. (2015) The Sun-Earth connect 3. *SpringerPlus* 4:285

Basilevsky, A.T., Head, J.W. (2000) Geologic Units on Venus: Evidence for Their Global Correlation. *Planet. Space Sci.* 48(12):75-111

Bulow, R.C., Johnson, C.L., Bills, B.G., Shearer, P.M. (2007) Temporal and spatial properties of some deep moonquake clusters. *J. Geophys. Res.* 112:E09003

Cazenave, A., Dobrovolskis, A., Lago, B. (1980) Orbital history of the Martian satellites with inferences on their origin, *Icarus* 44(3):730-744

Den Hartog, J. (1985). *Mechanical Vibrations* (4th ed.) Dover Publications, USA

Erlykin, A.D., Harper, D.A.T., Sloan, T., Wolfendale, A.W. (2017) Mass extinctions over the last 500 myr: An astronomical cause? *Palaeontol.* 60(2):159–167

Godfrey, D.A. (1988) A hexagonal feature around Saturn's north pole. *Icarus* 76(2):335-356

Jacoby, W.R. (2001) Successes and failures in geodynamics: from past to future. *J. Geodyn.* 32:3–27

Khan, A., Pommier, A., Neumann, G.A. (2013) The lunar moho and the internal structure of the Moon: A geophysical perspective. *Tectonophysics* 609:331-352

Lasser, J. (2019) *Geophysical Pattern Formation of Salt Playa*. Ph.D. dissertation, Division of Mathematics and Natural Sciences, University of Goettingen, Germany, pp. 200

Lorenz, R.D., Panning, M. (2018) Empirical recurrence rates for ground motion signals on planetary surfaces. *Icarus* 303:273–279

Fahnestock, E.G., Scheeres, D.J. (2008) Dynamical Characterization and Stabilization of Large Gravity-Tractor Designs. *J Guid. Control Dyn.* 31(3):501-521

Melosh, H.J. (1996) *Impact Cratering: A Geologic Process*. Oxford University Press, pp.245

Nakamura, Y., Professor Emeritus of Selenophyics, University of Texas at Austin. *Personal Communication*. 27-28 March 2019

Nakamura, Y., Latham, G.V., Dorman, H.J., Harris, J.E. (1981) *Passive Seismic Experiment, Long Period Event Catalog, Final Version*. Institute for Geophysics, University of Texas at Austin

Omerbashich, M. (2004) *Earth-model discrimination method*. Ph.D. Dissertation. ProQuest, pp.129

Omerbashich, M. (2006) Gauss-Vaníček Spectral Analysis of the Sepkoski Compendium: No New Life Cycles. *Comp. Sci. Eng.* 8:26-30

Omerbashich, M. (2007) Magnification of mantle resonance as a cause of tectonics. *Geod. Acta* 20(6):369-383

Omerbashich, M. (2008) Stochastic resonance for exploration geophysics. arXiv:0810.5708

Omerbashich, M. (2019a) Earth body resonance. *J. Geophys.* 63(1):15-29

Omerbashich, M. (2019b) On solar origin of alleged mass-extinction periods in records of natural data. (A.Y. Rozanov, Ed.) *Paleontol. J.* In press

Otto, K.A. et al. (2016) Origin and distribution of polygonal craters on Ceres. *Proceedings of 47th Lunar & Planetary Science Conference*, Houston TX, USA

Pikovsky, A., Rosenblum, M., Kurths, J. (2001) *Synchronization: A Universal Concept in Nonlinear Sciences* (Vol. 12). Cambridge University Press

Press, W.H., Teukolsky, S.A., Vetterling, W.T., Flannery, B.P. (2007) *Numerical Recipes: The Art of Scientific Computing* (3rd ed.). Cambridge University Press

Seidelmann, P. (1992) *Explanatory Supplement to the Astronomical Almanac. A revision to the Explanatory Supplement to the Astronomical Ephemeris and the American Ephemeris and Nautical Almanac*. Mill Valley, CA, USA. University Science Books

Smith, A.B. (2007) Marine diversity through the Phanerozoic: problems & prospects. (Bicentennial Review.) *J. Geol. Soc.* 164(4):731-745

Stevenson, D.J. (1983) Planetary magnetic fields. *Rep. Prog. Phys.* 46:555-620

Stevenson, D.J. (2008) A planetary perspective on the deep Earth. *Nature* 451:261-265

Strom, R.G., Schaber, G.G., Dawson, D.D. (1994) The global resurfacing of Venus. *J. Geophys. Res.* 99(E5):10899-10926

Thévenin, J., Romanelli, M., Vallet, M., Brunel, M., Erneux, T. (2011) Resonance Assisted Synchronization of Coupled Oscillators: Frequency Locking without Phase Locking. *Phys. Rev. Let.* 107:104101-1-5

Tse, D.P., Rucklidge, A.M., Hoyle, R.B., Silber, M. (2000) Spatial period-multiplying instabilities of hexagonal Faraday waves. *Physica D: Nonlin. Phenom.* 146(1-4):367-387

Van Dijk, T., Kistemaker, J. (1981) A New Explanation for the Hexagonal Shape of Lunar Craters. *Z. Naturforsch.* 36a:410-412

Vaníček, P. (1969) Approximate Spectral Analysis by Least-Squares Fit. *Astrophys. Space Sci.* 4(4):387–391

Vaníček, P. (1971) Further Development and Properties of the Spectral Analysis by Least-Squares Fit. *Astrophys. Space Sci.* 12(1):10–33

Yang, J.H., Sanjuán, M.A.F., Liu, H.G. (2016) Vibrational subharmonic and superharmonic resonances. *Comm. Nonlin. Sci. Num. Sim.* 30(1-3):362–372

Yin, A. (2012) Structural analysis of the Valles Marineris fault zone: Possible evidence for large-scale strike-slip faulting on Mars. *Lithosphere* 4(4):286–330.